PCCP

Accepted Manuscript

ROYAL SOCIETY OF CHEMISTRY

www.rsc.org/pccp

Microsolvation of $LiBO_2$ in Water: Anion Photoelectron Spectroscopy and *ab initio* Calculations

Zhen Zeng,[1] Gao-Lei Hou,[1] Jian Song,[2] Gang Feng,[1,*] Hong-Guang Xu,[1] Wei-Jun Zheng[1,*]

[1]*Beijing National Laboratory for Molecular Sciences, State Key Laboratory of Molecular Reaction Dynamics, Institute of Chemistry, Chinese Academy of Sciences, Beijing 100190, China*

[2] *Department of Physics, Henan Normal University, Henan, 453007, China*

* Corresponding author. E-mail: zhengwj@iccas.ac.cn; fenggang@iccas.ac.cn

Tel: +86 10 62635054, Fax: +86 10 62563167

Abstract

The microsolvation of $LiBO_2$ in water was investigated by conducting anion photoelectron spectroscopy and *ab initio* studies on the $LiBO_2(H_2O)_n^-$ (n = 0-5) clusters. By comparing calculations with experiments, the structures of these clusters and their corresponding neutrals were assigned, and their structural evolutions were revealed. During the anionic structural evolution with n increasing to 5, hydroxyborate and metaborate channels were identified and the metaborate channel is more favorable. For the hydroxyborate structures, the anionic Li^+-BO_2^- ion pair reacts with water molecule to produce $LiBO(OH)_2^-$ moiety and three water molecules tend to dissolve this moiety. In the metaborate channel, two types of solvent-separated ion pair (SSIP) geometries were determined as ring-type and linear-type. The transition from contact ion pair (CIP) to ring-type of SSIP starts at n = 3, while that to linear-type of SSIP occurs at n = 4. In neutral $LiBO_2(H_2O)_n$ clusters, the first water prefers to react with the Li^+-BO_2^- ion pair to generate $LiBO(OH)_2$ moiety, analogous to the bulk crystal phase of α-$LiBO_2$ with two O atoms substituted by two OH groups. The Li-O distance in $LiBO(OH)_2$ moiety increases with increasing number of water molecules and abruptly elongates at n = 4. Our studies provide new insight on the initial dissolution of $LiBO_2$ salt in water at molecular level and may be correlated to the bulk state.

1. Introduction

Salts play important roles in the fields like electrochemistry,[1-3] atmospheric chemistry,[4-6] and biochemistry[7, 8], as well as in our daily life. Gas phase hydrated salt clusters offer a useful model for investigating the microsolvation of salts which could provide molecular level information to understand the initial process of salt dissolution. Two kinds of structural configurations named contact ion pair (CIP) and solvent-separated ion pair (SSIP) are suggested to be the key species that dominate the initial steps of microsolvation.[9] Experimental[10-17] and theoretical[18-24] investigations have been conducted to reveal the initial process of salt dissolution, especially interesting is how many water molecules are needed to separate a specific salt CIP into SSIP. Since the solvent molecules can significantly affect the electronic states of salt ion pair, the evolution of salt electronic states with increasing number of water molecules can be probed by using anion photoelectron spectroscopy (PES). Interesting results have been obtained for several salts by anion PES combined with theoretical calculations. For example, the dissolution of $NaSO_4^-$ by water was studied by Wang et al.[25] Recently, our group investigated the microscopic solvation of $NaBO_2$,[26] MI (M = Li, Cs)[27] and NaCl trimer in water.[28]

Metaborate (BO_2^-) is a popular and important boron oxide anion and has been extensively studied both experimentally and theoretically.[29-34] BO_2 acts as a superhalogen[29] and its corresponding metaborate complexes such as $Au_n(BO_2)$,[35] $Cu_n(BO_2)_m^-$,[36] $Fe_nBO_2^-$,[37, 38] $Mn(BO_2)_n$,[39] $Al(BO_2)_n$,[40] and $Ag_n(BO_2)_m$[41, 42] have been investigated by experiments and theoretical calculations. Alkali metaborate can be considered as superhalogen salt analogous to alkali halides. So far, very little is known on the dissolution process of metaborate salt except for the $NaBO_2$.[26] Lithium metaborate is an important alkali metaborate. $LiBO_2$ melt is widely used as flux or chemical modifier[43-48] due to its low melting point, favorable dissolvability, high SHG coefficient,[49] high hardness and preventing from transition-metal contamination.[50] Aside from $LiBO_2$ melt, nanostructurisation of $LiBO_2$ can be utilized in ion conductors, battery systems, fuel cells or sensors[51, 52] because of the Li ion conductivity.

Lithium metaborate solid has different types of phases, mainly existing as α-$LiBO_2$, γ-$LiBO_2$ and amorphous $LiBO_2$, which changes along with environment variation.[53-56] Different increased temperature and dehydration rate allowed emergence of diverse phases of $LiBO_2$. $LiBO_2 \cdot 2(H_2O)$ can arise from the baking of $LiBO_2 \cdot 8(H_2O)$ below 140 ^oC and be

dehydrated to amorphous intermediate phase above 140 ^{o}C. The amorphous phase is formed at about 190 ^{o}C. However, the previous studies on the thermal dehydration products of $LiBO_2 \cdot 8(H_2O)$ crystal remain controversy,[57-60] especially regarding the water content of the amorphous phase after heating at 190 ^{o}C.

We here investigated $LiBO_2(H_2O)_n$ by conducting anion photoelectron spectroscopy and theoretical calculations, which may provide information for understanding the microsolvation process of $LiBO_2$ and the dehydration properties in hydrated condensed phase. By comparison with the hydrated $NaBO_2^-$,[26] apart from the evolution of ion pair from CIP to SSIP type of structure, the intracluster reaction will also be explored during the hydration of $LiBO_2^-$.

2. Experimental and computational methods

2.1 Experimental methods

The experiments were conducted on a home-built apparatus consisting of a time-of-flight mass spectrometer and a magnetic-bottle photoelectron spectrometer which has been described previously.[61] Briefly, the $LiBO_2(H_2O)_n^-$ clusters were produced in a laser vaporization source by ablating a rotating and translating $LiBO_2$ disc target with the second harmonic (532 nm) light pulses of an Nd:YAG laser, while helium carrier gas with 4 atm backing pressure seeded with water vapor was allowed to expand through a pulsed valve for generating hydrated $LiBO_2$ cluster anions and for cooling the formed clusters. The cluster anions were mass-analyzed by the time-of-flight mass spectrometer. The $LiBO_2(H_2O)_n^-$ (n = 1-5) anions were each mass-selected and decelerated before being photodetached by 1064 nm (1.165 eV) and 532 nm (2.331 eV) photons from another Nd: YAG laser. The photodetached electrons were collected and energy-analyzed by the magnetic-bottle photoelectron spectrometer. The photoelectron spectra were calibrated using the spectra of Cs^- and Bi^- taken at similar conditions. The instrumental resolution was ~40 meV for electrons with 1 eV kinetic energy.

2.2 Computational methods

The Gaussian09[62] program package was used for all the calculations. The structures of $LiBO_2(H_2O)_n^-$ (n = 0-5) clusters and their neutrals were optimized using density functional theory method at B3LYP[63, 64] functional and 6-311++G(d,p) basis set level. No symmetry

constraint was employed during the optimization. Natural bond orbital (NBO) analysis was performed based on the same functional and basis set. Harmonic vibrational frequencies were calculated to make sure that the obtained structures are the real local minima. The vibrational frequencies reported in the text were scaled by a factor of 0.9688 which is recommended for use with B3LYP/6-311++G(d,p) computations.[65] In order to obtain more accurate energies of $LiBO_2(H_2O)_n^{-/0}$ (n = 0-5), single-point energy calculations were conducted using CCSD(T) method[66] with the same basis set. All the calculated energies except the vertical detachment energies (VDEs) have been corrected by the zero-point vibrational energies. For further examination of the above results, the structures of $LiBO_2(H_2O)_n^-$ (n = 1-5) clusters and the corresponding neutrals were also optimized employing ωB97XD[67] functional and 6-31++G(d,p) basis set, which gave consistent results as B3LYP and are provided in the Supporting Information.

3. Experimental results

3.1 Mass spectra

The typical mass spectrum of the cluster anions is displayed in Figure 1. We could produce $LiBO_2(H_2O)_n^-$ cluster anions with up to 5 water molecules. The mass peak assignments were confirmed by analysis of the isotope abundance of B (19.9 % for ^{10}B, 80.1 % for ^{11}B). $LiBO_2(OH)(H_2O)_{n-1}^-$ anions (one mass unit less than the corresponding $LiBO_2(H_2O)_n^-$ clusters) may present in the experiments and perturb the isotope abundances of $LiBO_2(H_2O)_n^-$ (n = 1-5). However, we were able to clearly mass-select the $LiBO_2(H_2O)_n^-$ anions and recorded their photoelectron spectra without the contamination from $LiBO_2(OH)(H_2O)_{n-1}^-$. Besides, the VDEs of $LiBO_2(OH)(H_2O)_{n-1}^-$ anions are higher than the photon energies used in our experiments.

3.2 Photoelectron spectra

The photoelectron spectra of $LiBO_2(H_2O)_n^-$ (n = 0-5) recorded with 1064 and 532 nm photons are presented in Figure 2. The VDEs and the adiabatic detachment energies (ADEs) of $LiBO_2(H_2O)_n^-$ (n = 0-5) clusters were summarized in Table 1. Considering the broadening of the photoelectron spectra due to the instrumental resolution, the ADEs were estimated by adding the value of the instrumental resolution to the electron binding energies (EBEs) at the crossing points between the baseline and the leading edge of the first peaks. The VDEs were

measured from the maxima of the corresponding peaks.

In Figure 2, the 1064 nm spectrum of $LiBO_2^-$ displays two sharp peaks centered at 0.83 and 0.93 eV, respectively. These peaks are spaced by 810 ± 80 cm^{-1} which can be assigned to the Li-O stretching of neutral $LiBO_2$ by referring to the experimental frequency of LiO radical in the 720 to 850 cm^{-1} range.[68] The ADE and VDE of $LiBO_2^-$ are both estimated to be 0.83 eV based on the first peak (X) in the 1064 nm spectrum. In addition, the ADE of $LiBO_2^-$ corresponds to the electron affinity (EA) of neutral $LiBO_2$.

The resolved main feature (X) of $LiBO_2(H_2O)^-$ centered at 0.74 and 0.83 eV can be ascribed to the vibrational progression of neutral $LiBO_2(H_2O)$ with a frequency of 730 ± 80 cm^{-1}. Another feature at around 1.17 eV shows up in the 532 nm spectrum, higher than the feature X by ~0.41 eV (3310 cm^{-1}), close to the O-H stretch frequency of water molecule.

The main feature (X) of $LiBO_2(H_2O)_2^-$ centered at 0.86 and 0.97 eV and a broad shoulder (X') centered at 0.54 eV appears. The feature at 1.29 eV is higher than the peak X by ~0.43 eV (3470 cm^{-1}) and can also be assigned to the O-H stretching of water molecule, similar to the case of $LiBO_2(H_2O)^-$.

The spectra of $LiBO_2(H_2O)_3^-$ are distinct from those of $LiBO_2(H_2O)_{0\text{-}2}^-$. They show a broad major feature (X') centered at 0.50 eV. The spectrum recorded with 532 nm photons exhibits one weak feature (X) at 0.92 eV. For $LiBO_2(H_2O)_4^-$, the 1064 nm spectrum also reveals a 0.57 eV broad feature (X') and a small tail between 0.75 and 0.90 eV. The spectra of $LiBO_2(H_2O)_5^-$ only show a broad feature (X') centered at 0.56 eV. In the spectra of $LiBO_2(H_2O)_{3\text{-}5}^-$, we observe the lower EBE peaks X' as the dominant ones, distinct from the higher EBE peaks X in those of $LiBO_2(H_2O)_{0\text{-}2}^-$, indicating significant structural change may start at n = 3.

Interestingly, we found that some spectra are experimental conditions dependent. They behave differently when the water vapor content is enhanced in the carrier gas. We have taken the spectra at the experimental condition with more water vapor in the gas line. These spectra are shown in Figure 3. It can be seen that the spectra of $LiBO_2^-$, $LiBO_2(H_2O)_2^-$ and $LiBO_2(H_2O)_5^-$ in Figure 3 are similar to those in Figure 2, however, the spectra of $LiBO_2(H_2O)^-$, $LiBO_2(H_2O)_3^-$ and $LiBO_2(H_2O)_4^-$ present variations due to the increase of water

vapor in the carrier gas. Specifically, for $LiBO_2(H_2O)^-$, two new small peaks centered at 0.53 and 0.64 eV appear. The space between these two small peaks is 890 ± 80 cm^{-1}, which can be tentatively attributed to the vibrational progression of a low-lying isomer. For $LiBO_2(H_2O)_3^-$, the intensity of feature X increases due to the increasing of water vapor pressure at this experimental condition. For $LiBO_2(H_2O)_4^-$, in addition to the peak X', the spectrum recorded with 1064 nm photons shows some peaks similar to the peaks X in those of $LiBO_2(H_2O)_{0\text{-}2}^-$ with worse vibrational resolution, centered at 0.79 and 0.89 eV respectively. The 532 nm spectra of $LiBO_2(H_2O)_4^-$ at two experimental conditions are rather similar probably due to the broadening of the peaks and the low cross-section of the second and third peaks at 532 nm.

4. Theoretical results

The typical low-lying isomers of $LiBO_2(H_2O)_n^-$ (n = 0-5) clusters and their neutrals are summarized in Figures 4 and 5, respectively. More isomers were provided in the Supporting Information. The relative energies, ADEs and VDEs of these low-lying isomers are summarized and compared with the experimental values in Table 2.

4.1 $LiBO_2^-$ and $LiBO_2$

As shown in Figure 4, the most stable structure of $LiBO_2^-$ (0A) is linear with the Li atom binding to the BO_2 moiety through Li-O bond (1.73 Å). The calculated VDE (0.86 eV) of isomer 0A is in good accordance with the experimental value (0.83 eV).

The neutral $LiBO_2$ (0a) shown in Figure 5 is also linear but with shorter Li-O distance compared to that of the anion. The calculated Li-O stretching frequency is about 693 cm^{-1} after scaling, which is in reasonable agreement with our experimental value of 810 ± 80 cm^{-1} and other experimental observation in the region of 720 to 850 cm^{-1}.[68]

4.2 $LiBO_2(H_2O)^-$ and $LiBO_2(H_2O)$

In the lowest energy isomer of $LiBO_2(H_2O)^-$ (1A), the water molecule is connected to the Li atom via its O atom. The arrangement of O-Li-O is linear and the structure of BO_2 moiety is similar to that of $LiBO_2^-$. Compared to bare $LiBO_2^-$, the Li-O distance between the Li atom

and the O atom of the BO_2 moiety is unchanged (1.73 Å). The theoretical VDE of isomer 1A is 0.69 eV, in good agreement with the experimental VDE (0.74 eV) of peak X. The geometry of isomer 1B is a hydroxyborate type of structure, in which the O atom of water molecule is bound to the B atom with one H atom transferring to the oxygen atom of the BO_2 moiety. That means the B atom attaches to two OH groups and one O atom, with the O atom bonding to the Li atom. Isomer 1B can be recognized as $LiBO(OH)_2^-$, in which the metaborate Li^+-BO_2^- ion pair structure disappears and the B atom is tri-coordinated, resembling that in the bulk crystal phase of α-$LiBO_2$.[53, 56] (α-$LiBO_2$ contains endless chains of BO_3 triangles bonded by Li-O bonds). The relative energy of isomer 1B is 0.13 eV and its VDE (0.43 eV) is close to that of the lower EBE peak X' (0.53 eV) in Figure 3. Isomers 1C and 1D can be ruled out as their energies are much higher than that of 1A. Thus, isomer 1A is the dominating structure observed in the experiments and isomer 1B may be weakly populated and contributes to the band X'.

The most stable isomer of neutral $LiBO_2(H_2O)$ (1a) is similar to anionic 1B and can stand for the constituting motif of bulk crystal phase of α-$LiBO_2$[56] with two O atoms being substituted by two OH groups. The rocking vibrational frequency of the OH groups is calculated to be 913 cm^{-1} after scaling, consistent with the experimental observation of 890 ± 80 cm^{-1} related to peak X' in Figure 3. The second stable neutral (1b) is metaborate with circular ion pair structure, analogous to anionic 1C. The third sable neutral (1c) is similar to 1A with slight change of Li-O distance of Li^+-BO_2^- ion pair. The minor difference between the equilibrium geometries of the neutral and anionic states is consistent with the sharp and short vibrational progression of feature X in the 1064 nm spectrum. The calculated O-Li-O anti-symmetric stretching frequency of neutral 1c is 738 cm^{-1} after scaling, in good agreement with the experimental value of 730 ± 80 cm^{-1} related to peak X. In addition, the symmetric stretching and anti-symmetric stretching of H_2O in 1c are calculated and scaled to be 3699 and 3782 cm^{-1} respectively, accordant with the observation of 1.17 eV peak.

4.3 $LiBO_2(H_2O)_2^-$ and $LiBO_2(H_2O)_2$

For $LiBO_2(H_2O)_2^-$, the most stable isomer (2A) is evolved from the hydroxyborate isomer 1B with the second water molecule interacting with the Li atom, in the form of $LiBO(OH)_2(H_2O)^-$. The calculated VDE of isomer 2A is 0.40 eV, close to the experimental value of feature X' (0.55 eV). Degenerate in energy with 2A, isomer 2B also exhibits

tri-coordinated B atom and transferred H atoms, in the form of $Li(OH)B(OH)_3^-$. There is one OH group bridging between Li and $B(OH)_3$. The theoretical VDE (0.83 eV) of isomer 2B agrees well with that of peak X (0.86 eV). Derived from isomer 1C, isomer 2C has a metaborate structure with a 6-member ring consisting of the entire BO_2 moiety, Li atom and an OH group of one water molecule. The O-Li-O arrangement is non-linear ($\angle OLiO = 103°$) and the Li-O bond of Li^+-BO_2^- ion pair is elongated by 0.13 Å, comparing to that of 1A. Its theoretical VDE of 0.42 eV reasonably agrees with the experimental result of peak X' (0.55 eV). Isomer 2D has both two water molecules binding to the Li atom and its calculated VDE is 0.67 eV, close to the experimental result. Isomer 2E is less stable than 2C by 0.11 eV. It is derived from 1A with the second water molecule forming hydrogen bond (H-bond) with the terminal O atom of the BO_2 moiety. The linear Li^+-BO_2^- ion pair distance hardly changes comparing to that of 1A. Its theoretical VDE (0.81 eV) is in good accordance with the experimental VDE (0.86 eV) estimated from peak X. The calculated VDE of isomer 2F disagrees with the experimental one. Isomer 2G has much higher relative energy than that of metaborate isomer 2C and therefore cannot be populated in our experiments. Thus, isomers 2B and 2E are the most probable ones contributing to the higher EBE peak X, whereas 2A and 2C most likely dedicate to the lower EBE peak X'. Isomer 2D may contribute to the overlapped feature of X and X'. The experimental spectrum of $LiBO_2(H_2O)_2^-$ did not change significantly with the increase of water vapor pressure probably because the spectral features of the hydroxyborate and metaborate types of structures overlap with each other.

The lowest lying neutral isomer (2a) is similar to anionic 2A in the form of $LiBO(OH)_2(H_2O)$. Its Li-O bond length in the $LiBO(OH)_2$ moiety changes slightly by comparing to that of neutral 1a. The geometry of neutral 2b is metaborate and circular, analogous to that of 1b by interacting with the second water molecule through Li-O bond. Its Li-O distance of Li^+-BO_2^- ion pair is elongated by 0.21 Å compared to that of 1b. Isomer 2c is analogous to anionic 2B with LiOH residing at different position. Isomer 2d is an 8-member ring constituted by the Li atom, BO_2 moiety and two OH groups of two water molecules. The relative energy of isomer 2e is significantly higher than that of isomer 2b, indicating that the ring-type geometry is energetically more favorable than the linear-type one for the metaborate neutrals. The symmetric stretching and anti-symmetric stretching of two waters in neutral isomer are calculated to confirm the observation of 1.29 eV feature in the spectrum recorded with 532 nm photons.

4.4 $LiBO_2(H_2O)_3^-$ and $LiBO_2(H_2O)_3$

The most stable isomer of $LiBO_2(H_2O)_3^-$ (3A) also a hydroxyborate type of structure which can be developed from isomer 2B with the third water molecule interacting with the Li atom in the form of $Li(OH)B(OH)_3(H_2O)^-$. The calculated VDE of isomer 3A is 0.65 eV, in reasonable agreement with the experimental value of peak X' (0.50 eV). The relative energy of isomer 3B is 0.21 eV and its geometry is metaborate and circular, evolved from isomer 2C by binding the third water molecule to the BO_2 moiety and forming H-bond to the adjacent water molecule. Its Li-O bond length of Li^+-BO_2^- ion pair is comparable to that of isomer 2C. The calculated VDE (0.40 eV) of isomer 3B reasonably fits the experimental measurement of peak X'. Another hydroxyborate isomer 3C is formed by attaching the third water molecule to the Li atom based on 2A, in the form of $LiBO(OH)_2(H_2O)_2^-$. The theoretical VDE (0.39) of isomer 3C is close to that of peak X', however, it is less stable than the most stable hydroxyborate isomer 3A by 0.24 eV. Metaborate isomer 3D shows circular geometry while the contact between the Li atom and the BO_2 moiety is broken to present SSIP with two water molecules bridging the Li atom and two O atoms of the BO_2 moiety. The distance between the Li atom and the nearest O atom of the BO_2 moiety is abruptly lengthened to 3.82 Å, significantly longer than those in the metaborate $LiBO_2(H_2O)_{0\text{-}2}^-$ clusters. It should be noticed that the ring-type of SSIP structure contains the entire BO_2 moiety for ring-member and its Li^+-BO_2^- ion pair exhibits no direct interaction. The calculated VDE of isomer 3D is 0.53 eV, in excellent agreement with that of peak X'. Linear isomer 3E is derived from isomer 2D with the third water molecule forming H-bonds with the other two water molecules. Its Li^+-BO_2^- ion pair distance hardly changes compared to those of isomers 2D and 2E. The theoretical VDE (0.72 eV) of isomer 3E is in reasonable agreement with that of the higher EBE peak X (0.92 eV). Isomer 3F has a linear-type of SSIP geometry and its calculated VDE (0.61 eV) is far from the experimental VDE of feature X. Isomer 3G is scarcely populated in our experiments due to its higher relative energy in comparison with that of isomer 3B. Based on the above analysis, isomers 3A, 3B and 3D are suggested to be the lower EBE feature X' carriers, while isomer 3E is the most probable structure detected in our experiments for the higher EBE feature X.

For $LiBO_2(H_2O)_3$ neutral, the first two isomers (3a and 3b) show hydroxyborate structures in the forms of $LiBO(OH)_2(H_2O)_2$ and $Li(OH)B(OH)_3(H_2O)$ resembling anionic isomers 3C and 3A, respectively, with some structural deformations. For isomer 3a, the Li-O

bond length in the $LiBO(OH)_2$ moiety is increased by 0.15 Å compared to that of neutral 2a. Isomer 3c is a ring-type metaborate structure similar to 3B and can be derived from neutral 2b or 2d.

4.5 $LiBO_2(H_2O)_4^-$ and $LiBO_2(H_2O)_4$

The lowest-lying isomer of $LiBO_2(H_2O)_4^-$ (4A) is a hydroxyborate type of structure and can be viewed as developed from isomer 3A in which the Li atom is surrounded by three water molecules in the form of $Li(H_2O)_3BO(OH)_2^-$. Two water molecules separate the Li atom and $BO(OH)_2$ group. Its theoretical VDE (0.50 eV) agrees well with that of the lower EBE feature X' (0.57 eV). Isomer 4B is metaborate, circular and less stable than 4A by 0.42 eV. The Li^+-BO_2^- ion pair is separated by 3.38 Å and bridged by three water molecules. It belongs to ring-type of SSIP structure and its calculated VDE (0.38 eV) reasonably agrees with the experimental VDE (0.57 eV) of peak X'. Isomer 4C has a larger circular geometry based on 3B, in which the Li-O bond length of Li^+-BO_2^- ion pair changes slightly. The calculated VDE of isomer 4C is 0.40 eV, in reasonable accordance with the experimental measurement of peak X'. Isomer 4D is also circular and evolved from 3B with the fourth water molecule bonding to the titling O atom of the BO_2 moiety and the adjacent water molecule. The corresponding theoretical VDE is considerably low, which implies that it is difficult to generate anionic isomer 4D in our experiments. For isomer 4E, four water molecules surround the Li atom and two of them form H-bonds with the two oxygen atoms of the BO_2 moiety. It is a ring-type of SSIP structure and the distance between Li^+ and BO_2^- is 3.88 Å. The calculated VDE (0.64 eV) is in good agreement with the experimental VDE (0.57 eV) of feature X'. Isomer 4F is derived from hydroxyborate isomer 3C, in which the fourth water molecule forms one H-bond with one water molecule. It can be recognized as $LiBO(OH)_2(H_2O)_3^-$. The theoretical VDE (0.54 eV) of isomer 4F is close to that of peak X'. Isomer 4G is linear with four-coordinated Li atom separated from the BO_2 moiety by 3.43 Å. The theoretical VDE of isomer 4G is 0.76 eV, in excellent agreement with the experimental VDE (0.79 eV) of the higher EBE feature X. Interestingly, this is the first arising of linear-type of SSIP structure compared to the circular one. A larger ring-type of SSIP structure compared to 3D is formed for isomer 4H with large distance (3.58 Å) between salt ion pair. Isomers 4H and 4I are poorly populated in our experiments owing to their higher relative energies than that of 4B. Thus, the lower EBE feature X' can be mainly attributed to the isomers 4A, 4B, 4C and 4E, whereas the higher EBE peak X is most likely dedicated by the linear-type of SSIP 4G.

Two low-lying neutrals 4a and 4b have hydroxyborate configurations, similar to anionic 4A and 4D, respectively. For neutral 4a, the Li atom and $BO(OH)_2$ are separated by two water molecules with a distance of 3.02 Å. Metaborate neutral 4c is identical to 4D and its salt ion pair distance scarcely varies in comparison with that of neutral 3c.

4.6 $LiBO_2(H_2O)_5^-$ and $LiBO_2(H_2O)_5$

There are a large number of isomers and some of them coexist in our experiments for $LiBO_2(H_2O)_5^-$. Isomer 5A is a hydroxyborate type of structure and is derived from isomer 4A by inserting the fifth water molecule between the O atom and one water molecule in the form of $Li(H_2O)_3BO(OH)_2(H_2O)^-$. The Li atom is further separated from the $BO(OH)_2$ moiety by comparing with that of isomer 4A. The calculated VDE of isomer 5A (0.58 eV) is consistent with the experimental result (0.56 eV). Isomer 5B is metaborate and evolved from 4B with the fifth water molecule inserting between the O atom of the BO_2 moiety and the adjacent water molecule. Its calculated VDE (0.29 eV) is distinct from the experimental value. Isomer 5C is developed from isomer 4C with the fifth water molecule binding to both the dangling water and another in-ring water through two water-water H-bonds. The Li-O bond length of Li^+-BO_2^- ion pair is nearly unchanged in comparison with that of 4C. Its theoretical VDE of 0.50 eV is in good agreement with the experimental value. Isomer 5D can be seen as evolved from 4E by attaching the fifth water molecule only to the O atom of the BO_2 moiety. The calculated VDE (0.78 eV) is higher than the experimental value. Ring-type of SSIP structure 5E is also derived from 4E with a distance of 3.97 Å between Li^+-BO_2^- ion pair. Its calculated VDE (0.69 eV) is in reasonable accordance with the experimental VDE. Isomer 5F is a linear-type of SSIP developed from 4G with three water molecules separating the ion pair. The theoretical VDE of 0.81 eV is larger than the experimental one by 0.25 eV. Another linear-type of SSIP isomer 5G is also evolved from isomer 4G by binding the fifth water molecule to the terminal O atom of the BO_2 moiety via H-bond. Its calculated VDE (0.88 eV) is also far from the experimental value. Consequently, the broad feature in the spectrum of $LiBO_2(H_2O)_5^-$ is mainly contributed by isomers 5A, 5C and 5E, including hydroxyborate isomer and ring-type of SSIP structure. Isomers 5D, 5F and 5G may present to contribute to the tail of band. The experimental spectra of $LiBO_2(H_2O)_5^-$ did not change significantly with the increase of water vapor pressure probably because its spectral features are very broad and the spectral features of the hydroxyborate and metaborate types of structures overlap with

each other.

In the most stable isomer of neutral $LiBO_2(H_2O)_5$ (5a), the Li atom and $B(OH)_3$ group are separated by 3.25 Å via an OH group and three water molecules, larger than that in 4a by 0.23 Å. The energy gap of 0.39 eV between metaborate isomer 5c and hydroxyborate isomer 5a is greater than the corresponding tri-hydrate and tetra-hydrate neutrals.

5. Discussion

Overall, except for $LiBO_2^-$ and $LiBO_2(H_2O)^-$, the $LiBO_2(H_2O)_n^-$ (n = 2-5) cluster anions have the hydroxyborate isomers as the most stable geometries, indicating that the interaction of water with the Li atom and $BO(OH)_2^-$ can stabilize the hydroxyborate isomers. Two routines characterize the $LiBO_2(H_2O)_n^-$ anions structural evolution, identified as hydroxyborate and metaborate channels, as shown in Figure 6. In the hydroxyborate routine, the structure is evolved from $LiBO_2^-$ to $LiBO(OH)_2(H_2O)^-$ (n = 0-1) and from $Li(OH)B(OH)_3(H_2O)^-$ to $Li(H_2O)_3BO(OH)_2(H_2O)_n^-$ (n = 0-1). That means the Li^+-BO_2^- ion pair reacts with the first water molecule to generate the $LiBO(OH)_2^-$ moiety similar to that in the bulk crystal phase of α-$LiBO_2$. It is gradually dissolved with increased distance between Li and $BO(OH)_2$ as increasing number of water molecules. In the metaborate routine, the linear-type and ring-type geometries are identified. The geometric difference between them depends on whether the entire BO_2 moiety constituting into ring or not. Thus, the corresponding CIP and SSIP configurations can also be classified into two forms according to the linear and ring types of structures, respectively. During the metaborate geometric evolution process, the Li-O distance between the Li atom and the BO_2 moiety changes versus the number of water molecules, as plotted in Figure 7. It shows that the Li-O distance in the ring-type isomers increases abruptly when the $LiBO_2^-$ is hydrated by three water molecules. However, for the linear-type isomers, such dramatic elongation occurs with four water molecules. We notice that the elongation of Li-O distance from CIP to SSIP configuration in the ring-type structure is larger than that in the linear-type one. The hydroxyborate structures such as 2A, 3A, 4A and 5A are derived from isomer 1B. Isomer 1B has to be formed before isomers 2A-5A can be formed. Because the $LiBO(OH)_2^-$ moiety (1B) is higher in energy than the metaborate structure 1A of $LiBO_2(H_2O)^-$ by 0.13 eV, the hydroxyborate channel with increasing number of water molecules will be unfavorable, comparing to the metaborate channel. That is why the metaborate isomers could be significantly populated in our

experiments although they are higher in energy than the hydroxyborate type of structures. The higher EBE features (X) in the photoelectron spectra of $LiBO_2(H_2O)_n^-$ (n = 0-5) are mainly attributed to the metaborate linear-type isomers such as 0A, 1A, 2D, 2E, 3E and 4G (SSIP), while the lower EBE features (X') are mostly contributed by hydroxyborate isomers 1B, 2A, 3A, 4A, 5A and ring-type isomers like 2C, 3B, 3D (SSIP), 4B (SSIP), 4C, 4D, 4E (SSIP), 5C and 5E (SSIP), respectively. The results imply that the dissolution process depends not only on the number of water molecules but also on the intrinsic structures which are determined by the competition between ion-ion, ion-water and water-water interactions.

In neutral $LiBO_2(H_2O)_n$, the first water molecule prefers to react with $LiBO_2$ to generate $LiBO(OH)_2$, analogous to bulk crystal phase of α-$LiBO_2$ with two O atoms substituted by two OH groups. It is dissolved step by step with increasing number of water molecules. The structural evolution is presented in Figure 8 and the Li-O distance variation in $LiBO(OH)_2$ moiety versus the number of water molecules is shown in Figure 9. The distance elongates abruptly at n = 4. Note that the process for the formation of $LiBO(OH)_2(H_2O)_n$ can be considered as an intracluster reaction, which has been observed experimentally and theoretically in some ion-molecules clusters.[69-74] Here, the salt-water intracluster reaction was observed for the first time in $LiBO_2(H_2O)_n$.

From the natural bond orbital (NBO) charge distribution analysis, we found that the extra electron mostly localizes on the Li atom in bare $LiBO_2^-$ (from $Li^{+0.948}BO_2^{-0.948}$ of neutral to $Li^{-0.038}BO_2^{-0.962}$ of anion). During dissolution, the extra electron also partly localizes on the water molecule. When one water molecule is added, the EBE of feature X shifts toward lower value compared to that of $LiBO_2^-$. The spectral shift can be ascribed to the much stronger electrostatic interaction between the water molecule and Li atom in the neutral state in which the Li atom is more positively charged than that in the anionic state. This is similar to the cases of $LiI(H_2O)^-$[27] and $NaBO_2(H_2O)_3^-$.[26]

Here, we compare the structures of $LiBO_2(H_2O)_n^-$ with those of $NaBO_2(H_2O)_n^-$. In the most stable isomer of $LiBO_2(H_2O)^-$ (1A), the water molecule interacts with the Li atom. This is different from that of $NaBO_2(H_2O)^-$,[26] in which the water molecule interacts with BO_2 group via a O···H-O hydrogen bond. This implies that the water-Li interaction in $LiBO_2(H_2O)^-$ is stronger than the water-BO_2 interaction, while the water-Na interaction in $NaBO_2(H_2O)^-$ is weaker than the water-BO_2 interaction. In addition, the structural difference

between the $LiBO_2(H_2O)^-$ and $NaBO_2(H_2O)^-$ also coordinates with the difference between their photoelectron spectra, in which the photoelectron peak of $LiBO_2(H_2O)^-$ shifts toward lower EBE compared to that of $LiBO_2^-$ while the photoelectron peak of $NaBO_2(H_2O)^-$ shifts toward higher EBE compared to that of $NaBO_2^-$. When interacting with two or more water molecules, $LiBO_2^-$ prefers to react with H_2O and the Li^+-BO_2^- ion pair structure disappears. This hydroxyborate routine is absent in $NaBO_2(H_2O)_n^-$. For metaborate geometric evolution, the first SSIP is ring-type structure of $LiBO_2(H_2O)_3^-$ comparing to the linear-type of SSIP structure of $NaBO_2(H_2O)_3^-$. In neutral $LiBO_2(H_2O)_n$, the reaction between salt and the first water molecule happens immediately and more water molecules continue to dissolve the product of this reaction, while for $NaBO_2(H_2O)_n$, the Na^+ and BO_2^- ions are always in contact.

6. Conclusions

We conducted photoelectron spectroscopic study combined with *ab initio* calculations on the $LiBO_2(H_2O)_n^-$ (n = 0-5) clusters and their neutrals to reveal the microscopic solvation of $LiBO_2$ in water. Two structural evolution channels, namely the hydroxyborate and metaborate channels, are presented in the anionic solvation process and the metaborate channel is more favorable. The hydroxyborate structures are more stable than the metaborate ones for $n \geq 2$, indicating that the intracluster reaction is preferred to generate the bulk-like structure motif. For the hydroxyborate channel, the water molecules interact with the product ($LiBO(OH)_2^-$) originated from the intracluster reaction between $LiBO_2^-$ and the first water molecule. In the metaborate channel, two types of structures coexist. One type has almost linear Li-O-B-O arrangement and the other type forms circular geometry with bent Li-O-B structure. The Li-O distance of ion pair increases as the number of water molecules increases. Dramatic increasing of Li-O distance emerges at n = 4 in the linear configurations while the significant elongation of Li-O bond length appears at n = 3 for the ring-type of structures. The ion pair in the ring-type isomer is more separated than that in the linear-type one during the microsolvation process. For the most stable isomers of $LiBO_2(H_2O)_n$ neutrals, the ion pair starts to react with the first water molecule to form the proton transfer product, $LiBO(OH)_2$. Four water molecules can separate the Li atom and $BO(OH)_2$ group.

Acknowledgements

This work was supported by the Knowledge Innovation Program of the Chinese Academy of

Sciences (Grant No. KJCX2-EW-H01) and the Natural Science Foundation of China (Grant No. 21403249). The theoretical calculations were conducted on the ScGrid and DeepComp 7000 of the Supercomputing Center, Computer Network Information Center of Chinese Academy of Sciences.

References

1. Z. Zhang, X. Chen, F. Li, Y. Lai, J. Li, P. Liu and X. Wang, *J. Power Sources*, 2010, 195, 7397-7402.
2. G. Mamantov, in *Molten Salt Chemistry*, eds. G. Mamantov and R. Marassi, Springer Netherlands, 1987, vol. 202, ch. 12, pp. 259-270.
3. V. Aravindan, J. Gnanaraj, S. Madhavi and H.-K. Liu, *Chem. Eur. J.*, 2011, 17, 14326-14346.
4. E. M. Knipping, M. J. Lakin, K. L. Foster, P. Jungwirth, D. J. Tobias, R. B. Gerber, D. Dabdub and B. J. Finlayson-Pitts, *Science*, 2000, 288, 301-306.
5. S. W. Hunt, M. Roeselova, W. Wang, L. M. Wingen, E. M. Knipping, D. J. Tobias, D. Dabdub and B. J. Finlayson-Pitts, *J. Phys. Chem. A*, 2004, 108, 11559-11572.
6. K. W. Oum, M. J. Lakin, D. O. DeHaan, T. Brauers and B. J. Finlayson-Pitts, *Science*, 1998, 279, 74-76.
7. M. P. Apse, G. S. Aharon, W. A. Snedden and E. Blumwald, *Science*, 1999, 285, 1256-1258.
8. T. Cserhati and E. Forgacs, *Int. J. Pharm.*, 2003, 254, 189-196.
9. S. Winstein, E. Clippinger, A. H. Fainberg and G. C. Robinson, *J. Am. Chem. Soc.*, 1954, 76, 2597-2598.
10. A. Mizoguchi, Y. Ohshima and Y. Endo, *J. Am. Chem. Soc.*, 2003, 125, 1716-1717.
11. A. T. Blades, M. Peschke, U. H. Verkerk and P. Kebarle, *J. Am. Chem. Soc.*, 2004, 126, 11995-12003.
12. J.-J. Max and C. Chapados, *J. Chem. Phys.*, 2001, 115, 2664-2675.
13. Q. Zhang, C. J. Carpenter, P. R. Kemper and M. T. Bowers, *J. Am. Chem. Soc.*, 2003, 125, 3341-3352.
14. L. Partanen, M.-H. Mikkelä, M. Huttula, M. Tchaplyguine, C. Zhang, T. Andersson and O. Björneholm, *J. Chem. Phys.*, 2013, 138, 044301.
15. G. Grégoire, M. Mons, C. Dedonder-Lardeux and C. Jouvet, *Eur. Phys. J. D*, 1998, 1, 5-7.
16. A. Mizoguchi, Y. Ohshima and Y. Endo, *J. Chem. Phys.*, 2011, 135, 064307.
17. G. Grégoire, M. Mons, I. Dimicoli, C. Dedonder-Lardeux, C. Jouvet, S. Martrenchard and D. Solgadi, *J. Chem. Phys.*, 2000, 112, 8794-8805.
18. C. J. Fennell, A. Bizjak, V. Vlachy and K. A. Dill, *J. Phys. Chem. B*, 2009, 113, 6782-6791.
19. C.-K. Siu, B. S. Fox-Beyer, M. K. Beyer and V. E. Bondybey, *Chem. Eur. J.*, 2006, 12, 6382-6392.
20. D. E. Bacelo and Y. Ishikawa, *Chem. Phys. Lett.*, 2000, 319, 679-686.
21. A. C. Olleta, H. M. Lee and K. S. Kim, *J. Chem. Phys.*, 2006, 124, 024321.
22. S. Yamabe, H. Kouno and K. Matsumura, *J. Phys. Chem. B*, 2000, 104, 10242-10252.
23. A. Sen and B. Ganguly, *Theor. Chem. Acc.*, 2012, 131, 1-13.
24. D. E. Woon and T. H. Dunning, Jr., *J. Am. Chem. Soc.*, 1995, 117, 1090-1097.
25. X.-B. Wang, H.-K. Woo, B. Jagoda-Cwiklik, P. Jungwirth and L.-S. Wang, *Phys. Chem. Chem. Phys.*, 2006, 8, 4294-4296.
26. Y. Feng, M. Cheng, X.-Y. Kong, H.-G. Xu and W.-J. Zheng, *Phys. Chem. Chem. Phys.*, 2011, 13, 15865-15872.
27. R.-Z. Li, C.-W. Liu, Y. Q. Gao, H. Jiang, H.-G. Xu and W.-J. Zheng, *J. Am. Chem. Soc.*, 2013, 135, 5190-5199.
28. C.-W. Liu, G.-L. Hou, W.-J. Zheng and Y. Gao, *Theor. Chem. Acc.*, 2014, 133, 1-10.
29. H.-J. Zhai, L.-M. Wang, S.-D. Li and L.-S. Wang, *J. Phys. Chem. A*, 2007, 111, 1030-1035.
30. J. V. Ortiz, *J. Chem. Phys.*, 1993, 99, 6727-6731.
31. D. E. Jensen, *J. Chem. Phys.*, 1970, 52, 3305-3306.
32. V. G. Zakrzewski and A. I. Boldyrev, *J. Chem. Phys.*, 1990, 93, 657-660.
33. D. E. Jensen, *Trans. Faraday Soc.*, 1969, 65, 2123-2132.

34. R. D. Srivastava, O. M. Uy and M. Farber, *Trans. Faraday Soc.*, 1971, 67, 2941-2944.
35. M. Götz, M. Willis, A. K. Kandalam, G. F. Ganteför and P. Jena, *ChemPhysChem*, 2010, 11, 853-858.
36. Y. Feng, H.-G. Xu, W. Zheng, H. Zhao, A. K. Kandalam and P. Jena, *J. Chem. Phys.*, 2011, 134, 094309.
37. Y. Feng, H.-G. Xu, Z.-G. Zhang, Z. Gao and W. Zheng, *J. Chem. Phys.*, 2010, 132, 074308.
38. H. M. Zhao, X. Lin, Y. Li, Q. Wang and P. Jena, *Phys. Lett. A*, 2014, 378, 2959-2964.
39. P. Koirala, K. Pradhan, A. K. Kandalam and P. Jena, *J. Phys. Chem. A*, 2013, 117, 1310-1318.
40. G. L. Gutsev, C. A. Weatherford, L. E. Johnson and P. Jena, *J. Comput. Chem.*, 2012, 33, 416-424.
41. H. Chen, X.-Y. Kong, W. Zheng, J. Yao, A. K. Kandalam and P. Jena, *ChemPhysChem*, 2013, 14, 3303-3308.
42. X.-Y. Kong, H.-G. Xu, P. Koirala, W.-J. Zheng, A. K. Kandalam and P. Jena, *Phys. Chem. Chem. Phys.*, 2014, 16, 26067-26074.
43. K. He, D. He, L. Lei, Y. Zou, J. Qin and S. Wang, *Solid State Commun.*, 2010, 150, 2106-2108.
44. H. Kageyama, K. Onizuka, T. Yamauchi and Y. Ueda, *J. Cryst. Growth*, 1999, 206, 65-67.
45. R. W. Smith and D. A. Keszler, *J. Solid State Chem.*, 1991, 93, 430-435.
46. E. G. Moshopoulou, *J. Am. Ceram. Soc.*, 1999, 82, 3317-3320.
47. P. Motabar, K. G. W. Inn, J. Davis and J. LaRosa, *J. Radioanal. Nucl. Chem.*, 2009, 282, 335-341.
48. M. C. Santos, A. R. A. Nogueira and J. A. Nobrega, *J. Braz. Chem. Soc.*, 2005, 16, 372-380.
49. C. D. McMillen, H. G. Giesber and J. W. Kolis, *J. Cryst. Growth*, 2008, 310, 299-305.
50. M. M. Islam, T. Bredow and P. Heitjans, *J. Phys. Chem. C*, 2011, 115, 12343-12349.
51. P. Heitjans, E. Tobschall and M. Wilkening, *Eur. Phys. J.-Spec. Top.*, 2008, 161, 97-108.
52. A. Kuhn, E. Tobschall and P. Heitjans, *Z. Phys. Chemie-Int. J. Res. Phys. Chem. Chem. Phys.*, 2009, 223, 1359-1377.
53. L. Lei, D. He, K. He, J. Qin and S. Wang, *J. Solid State Chem.*, 2009, 182, 3041-3048.
54. A. Kirfel, G. Will and R. F. Stewart, *Acta Crystallogr. Sect. B-Struct. Sci.*, 1983, 39, 175-185.
55. M. Marezio and J. P. Remeika, *J. Phys. Chem. Solids*, 1965, 26, 2083-2085.
56. W. H. Zachariasen, *Acta Crystallogr.*, 1964, 17, 749-751.
57. J. K. Liang, X. L. Chen, J. R. Min, Z. Chai, S. Q. Zhao, X. R. Cheng, Y. L. Zhang and G. H. Rao, *Phys. Rev. B*, 1995, 51, 756-762.
58. E. Betourne and M. Touboul, *Powder Diffr.*, 1997, 12, 155-159.
59. N. Koga and T. Utsuoka, *Thermochim. Acta*, 2006, 443, 197-205.
60. M. Touboul, N. Penin and G. Nowogrocki, *Solid State Sci.*, 2003, 5, 1327-1342.
61. H.-G. Xu, Z.-G. Zhang, Y. Feng, J. Yuan, Y. Zhao and W. Zheng, *Chem. Phys. Lett.*, 2010, 487, 204-208.
62. M. J. Frisch, G. W. Trucks, H. B. Schlegel, G. E. Scuseria, M. A. Robb, J. R. Cheeseman, G. Scalmani, V. Barone, B. Mennucci, G. A. Petersson, H. Nakatsuji, M. Caricato, X. Li, H. P. Hratchian, A. F. Izmaylov, J. Bloino, G. Zheng, J. L. Sonnenberg, M. Hada, M. Ehara, K. Toyota, R. Fukuda, J. Hasegawa, M. Ishida, T. Nakajima, Y. Honda, O. Kitao, H. Nakai, T. Vreven, J. A. M. Jr., J. E. Peralta, F. Ogliaro, M. Bearpark, J. J. Heyd, E. Brothers, K. N. Kudin, V. N. Staroverov, R. Kobayashi, J. Normand, K. Raghavachari, A. Rendell, J. C. Burant, S. S. Iyengar, J. Tomasi, M. Cossi, N. Rega, J. M. Millam, M. Klene, J. E. Knox, J. B. Cross, V. Bakken, C. Adamo, J. Jaramillo, R. Gomperts, R. E. Stratmann, O. Yazyev, A. J. Austin, R. Cammi, C. Pomelli, J. W. Ochterski, R. L. Martin, K. Morokuma, V. G. Zakrzewski, G. A. Voth, P. Salvador, J. J. Dannenberg, S. Dapprich, A. D. Daniels, O. Farkas, J. B. Foresman, J. V. Ortiz, J. Cioslowski and D. J. Fox, *Gaussian 09, Revision A.02, Gaussian, Inc., Wallingford CT*, 2009.
63. A. D. Becke, *J. Chem. Phys.*, 1993, 98, 5648-5652.

64. C. Lee, W. Yang and R. G. Parr, *Phys. Rev. B*, 1988, 37, 785-789.
65. J. P. Merrick, D. Moran and L. Radom, *J. Phys. Chem. A*, 2007, 111, 11683-11700.
66. J. A. Pople, M. Head-Gordon and K. Raghavachari, *J. Chem. Phys.*, 1987, 87, 5968-5975.
67. J.-D. Chai and M. Head-Gordon, *Phys. Chem. Chem. Phys.*, 2008, 10, 6615-6620.
68. C. Yamada and E. Hirota, *J. Chem. Phys.*, 1993, 99, 8489-8497.
69. H. Watanabe and S. Iwata, *J. Phys. Chem.*, 1996, 100, 3377-3386.
70. T. J. Selegue and J. M. Lisy, *J. Am. Chem. Soc.*, 1994, 116, 4874-4880.
71. A. M. Ricks, A. D. Brathwaite and M. A. Duncan, *J. Phys. Chem. A*, 2013, 117, 11490-11498.
72. A. C. Harms, S. N. Khanna, B. Chen and A. W. Castleman, *J. Chem. Phys.*, 1994, 100, 3540-3544.
73. M. Beyer, E. R. Williams and V. E. Bondybey, *J. Am. Chem. Soc.*, 1999, 121, 1565-1573.
74. M. Beyer, C. Berg, H. W. Görlitzer, T. Schindler, U. Achatz, G. Albert, G. Niedner-Schatteburg and V. E. Bondybey, *J. Am. Chem. Soc.*, 1996, 118, 7386-7389.

Table 1 Experimental VDEs and ADEs of $LiBO_2(H_2O)_n^-$ (n = 0-5). All values are in eV.

Cluster	X'		X	
	ADE	VDE	ADE	VDE
$LiBO_2^-$			0.83	0.83
$LiBO_2(H_2O)^-$	0.46	0.53	0.71	0.74
$LiBO_2(H_2O)_2^-$	0.47	0.55	0.80	0.86
$LiBO_2(H_2O)_3^-$	0.38	0.50	0.73	0.92
$LiBO_2(H_2O)_4^-$	0.42	0.57	0.74	0.79
$LiBO_2(H_2O)_5^-$	0.33	0.56		

Table 2 Relative energies of the low energy isomers of $LiBO_2(H_2O)_n^-$ (n = 0-5) as well as the comparison of their theoretical VDEs and ADEs based on CCSD(T) // B3LYP/6-311++G(d,p) to the experimental measurements. All energies are in eV.

Isomer		ΔE	ADE		VDE	
			Theo.	Expt.	Theo.	Expt.
$LiBO_2^-$	0A	0.00	0.85	0.83	0.86	0.83
$LiBO_2(H_2O)^-$	1A	0.00	0.72	0.71	0.69	0.74
	1B	0.13	0.42	0.46	0.43	0.53
	1C	0.26	0.34		0.40	
	1D	0.28	0.99		1.04	
$LiBO_2(H_2O)_2^-$	2A	0.00	0.43	0.47	0.40	0.55
	2B	0.01	0.48	0.80	0.83	0.86
	2C	0.12	0.35		0.42	
	2D	0.14	0.51		0.67	
	2E	0.23	0.81		0.81	
	2F	0.28	0.25		0.29	
	2G	0.39	0.35		0.49	
$LiBO_2(H_2O)_3^-$	3A	0.00	0.31	0.38	0.65	0.50
	3B	0.21	0.29		0.40	
	3C	0.24	-0.16		0.39	
	3D	0.30	0.47		0.53	
	3E	0.37	0.72	0.73	0.72	0.92
	3F	0.38	0.64		0.61	
	3G	0.40	0.10		0.78	
$LiBO_2(H_2O)_4^-$	4A	0.00	0.46	0.42	0.50	0.57
	4B	0.42	0.30		0.38	
	4C	0.47	0.27		0.40	
	4D	0.49	0.09		0.12	
	4E	0.50	0.38		0.64	
	4F	0.50	0.01		0.54	
	4G	0.54	0.50	0.74	0.76	0.79
	4H	0.58	0.20		0.61	
	4I	0.60	0.19		0.64	
$LiBO_2(H_2O)_5^-$	5A	0.00	0.17	0.33	0.58	0.56
	5B	0.41	0.23		0.29	
	5C	0.48	0.45		0.50	
	5D	0.55	0.12		0.78	
	5E	0.55	0.16		0.69	
	5F	0.56	0.09		0.81	
	5G	0.57	0.09		0.88	
	5H	0.57	0.18		0.71	
	5I	0.60	0.27		0.40	

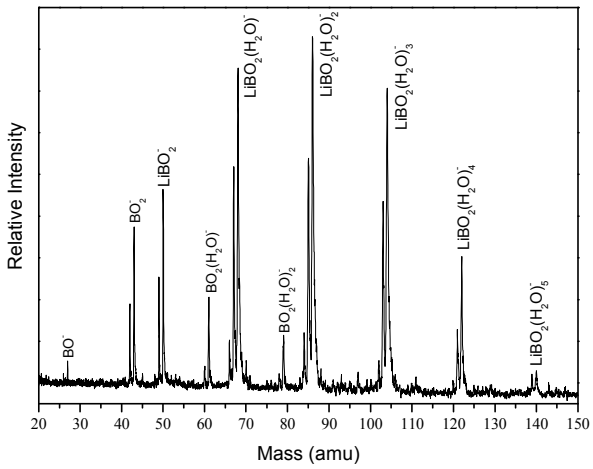

Figure 1 Mass spectrum of $LiBO_2(H_2O)_n^-$ (n = 0-5) cluster anions.

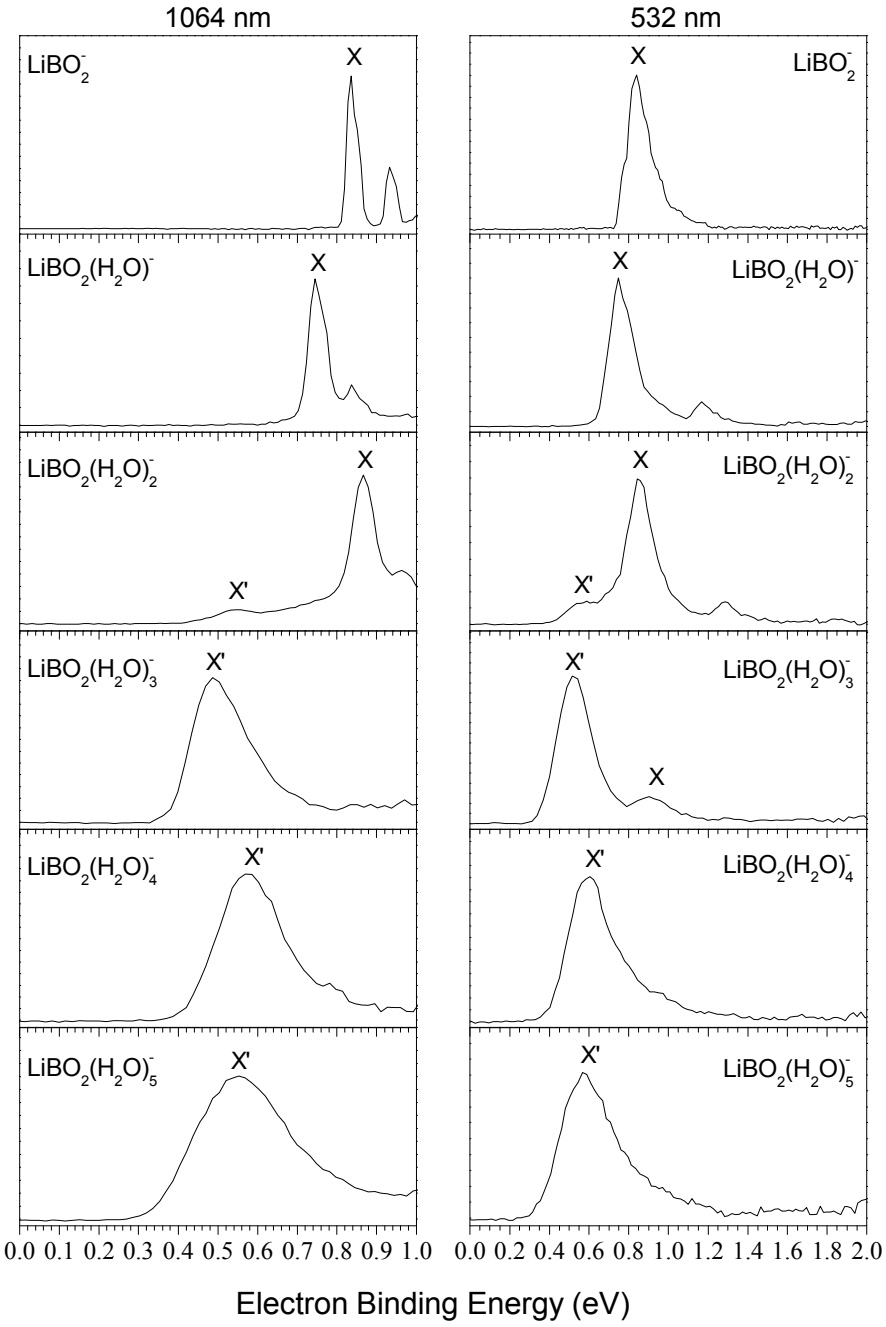

Figure 2 Photoelectron spectra of $LiBO_2(H_2O)_n^-$ (n = 0-5) recorded with 1064 and 532 nm photons.

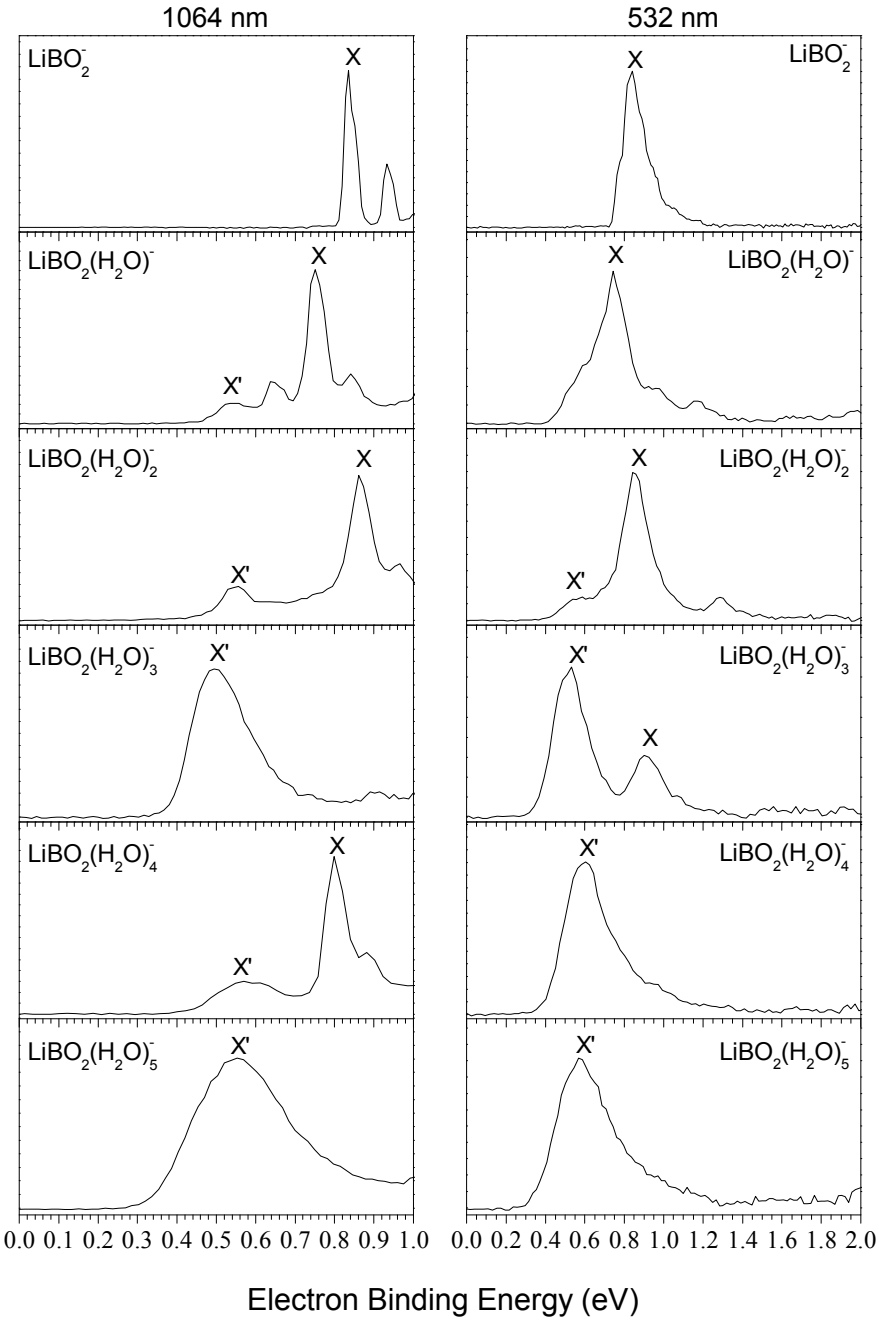

Figure 3 Photoelectron spectra of $LiBO_2(H_2O)_n^-$ (n = 0-5) recorded with 1064 and 532 nm photons. The $LiBO_2(H_2O)_n^-$ clusters were generated at the experimental condition with higher water vapor pressure in the gas line compared to those in Figure 2.

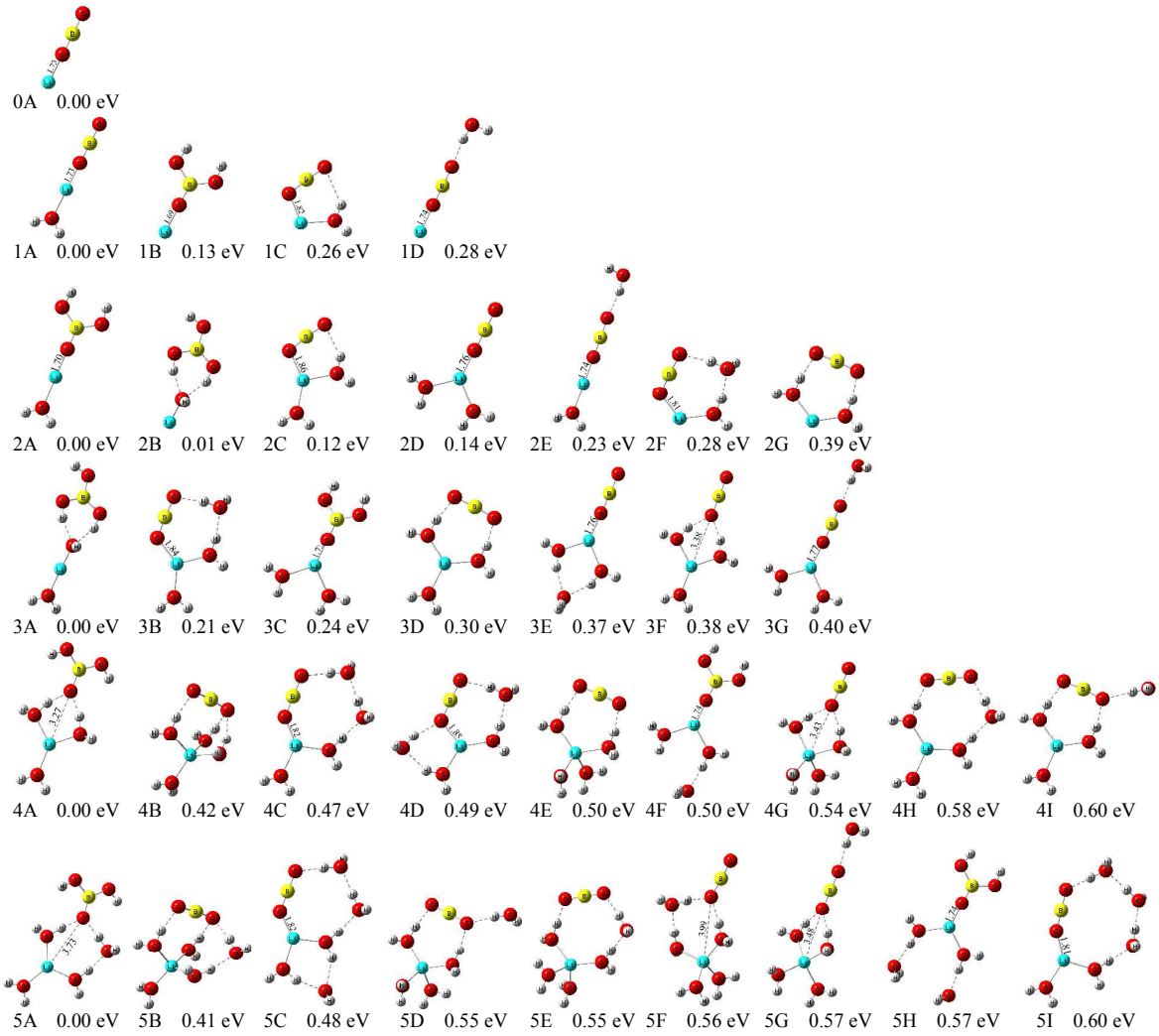

Figure 4 Optimized geometries of the typical low-lying isomers of $LiBO_2(H_2O)_n^-$ (n = 0-5) based on CCSD(T) // B3LYP/6-311++G(d,p). Relative energies and Li-O bond lengths (in Å) are indicated.

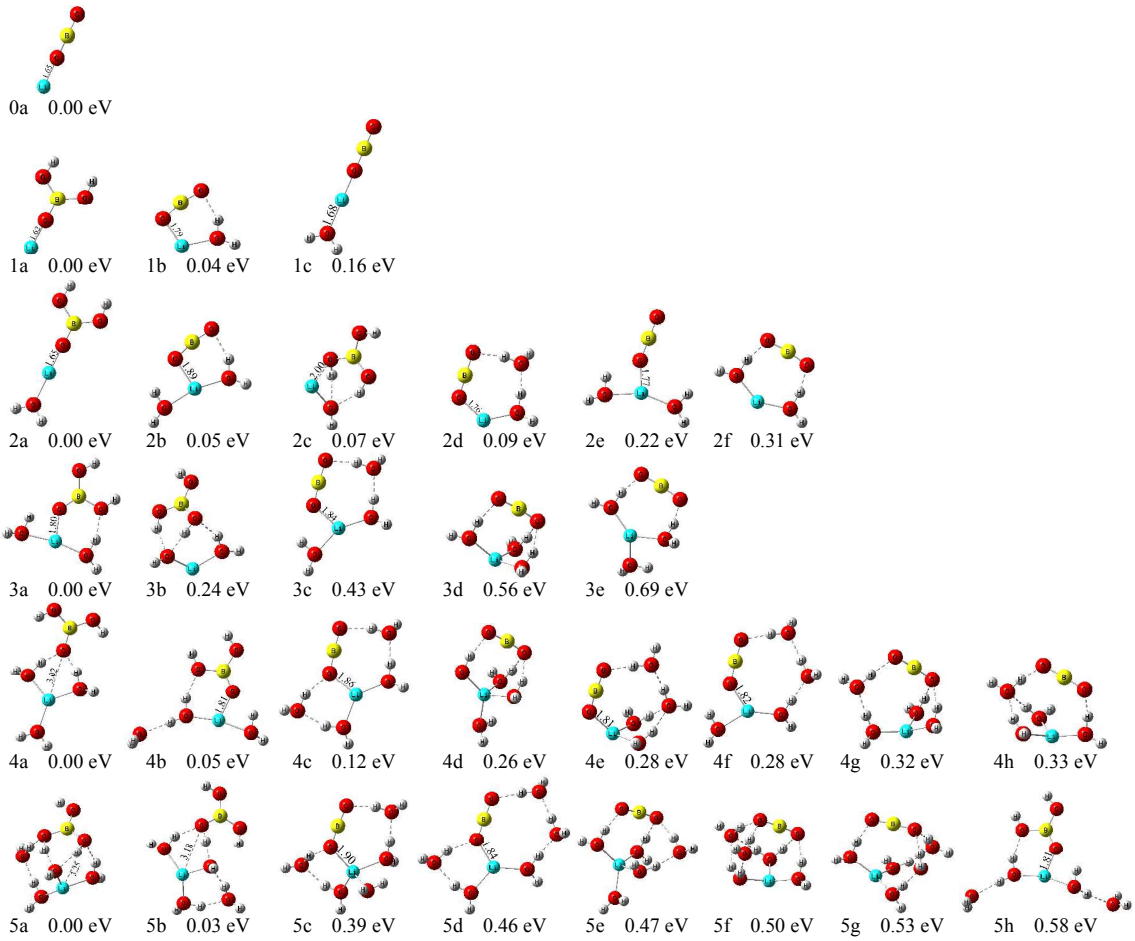

Figure 5 Optimized geometries of the typical low-lying isomers of $LiBO_2(H_2O)_n$ (n = 0-5) neutral clusters based on CCSD(T) // B3LYP/6-311++G(d,p). Relative energies and Li-O bond lengths (in Å) are indicated.

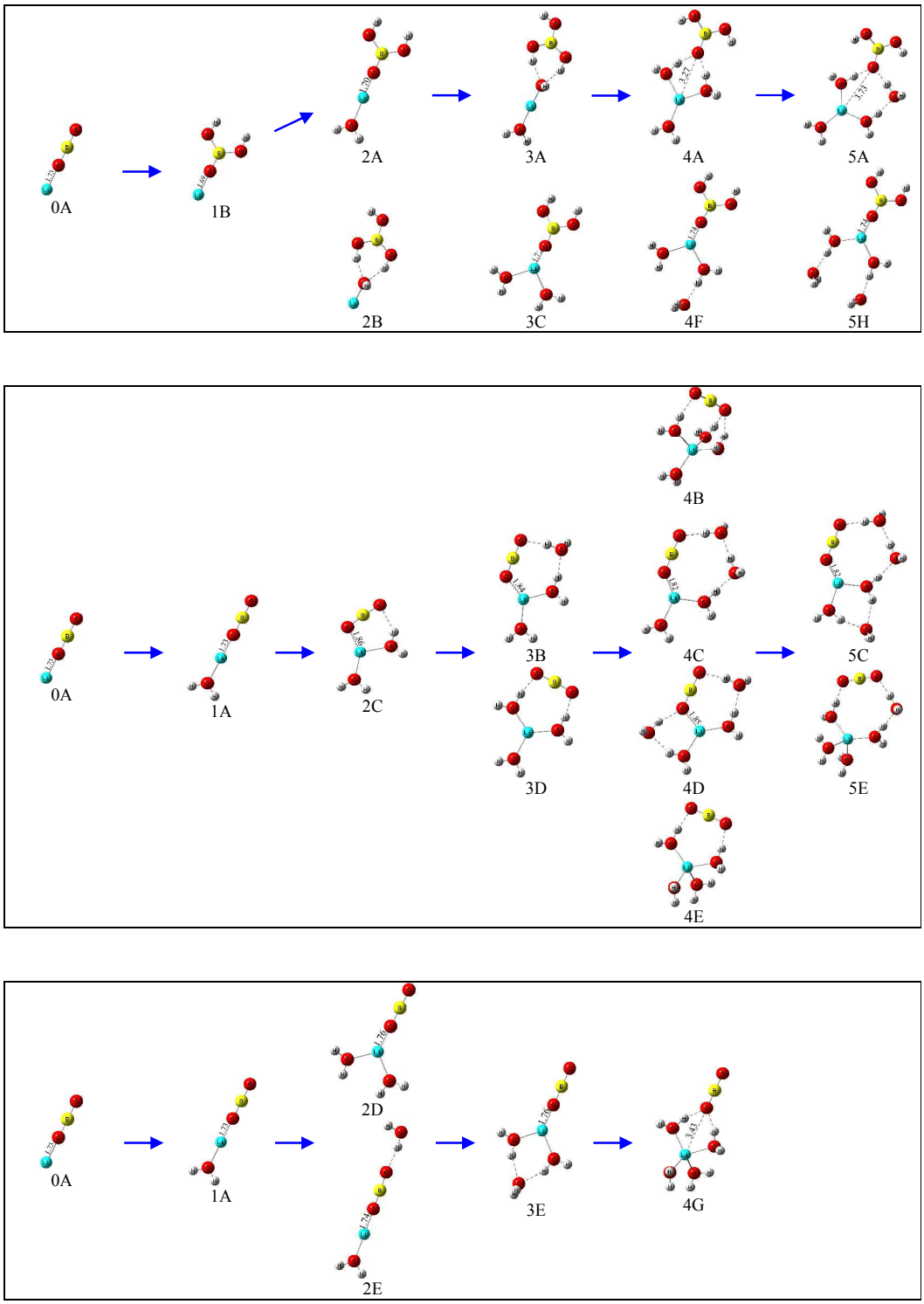

Figure 6 The structural evolution of $LiBO_2(H_2O)_n^-$ anions. The first row shows the hydroxyborate channel. The second and third rows show the metaborate channel.

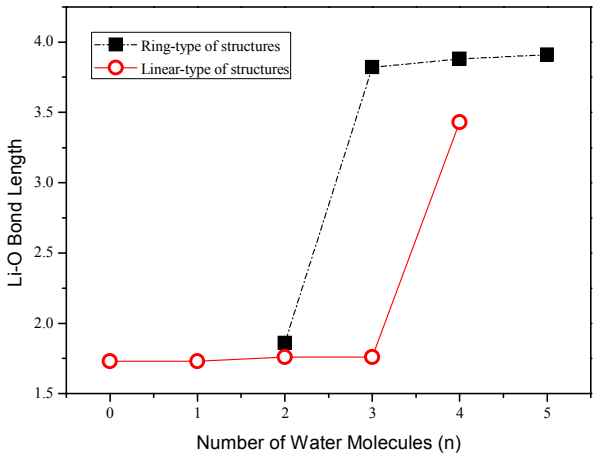

Figure 7 The variation of Li-O bond length in $LiBO_2(H_2O)_n^-$ with increasing number of water molecules for the metaborate channel. All above structures are the most probable ones in the experiments.

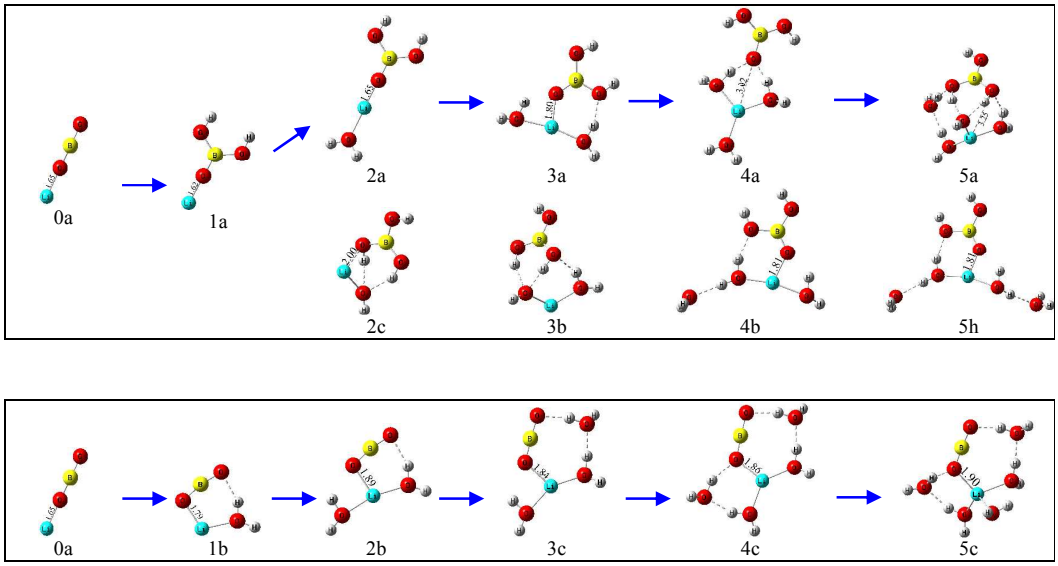

Figure 8 The structural evolution of neutral $LiBO_2(H_2O)_n$.

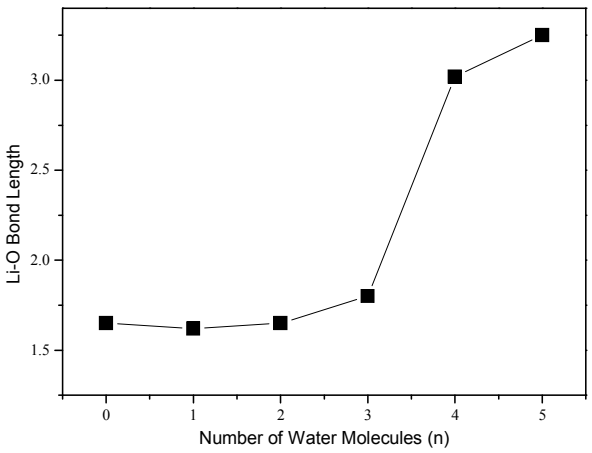

Figure 9 The variation of Li-O distance in $LiBO(OH)_2(H_2O)_{n-1}$ (n = 1-5) versus the number of water molecules.